Microstructural Control in Hot Working of IN-718 Superalloy Using Processing Map

N. SRINIVASAN and Y.V.R.K. PRASAD

The hot-working characteristics of IN-718 are studied in the temperature range 900 °C to 1200 °C and strain rate range 0.001 to 100 s^{-1} using hot compression tests. Processing maps for hot working are developed on the basis of the strain-rate sensitivity variations with temperature and strain rate and interpreted using a dynamic materials model. The map exhibits two domains of dynamic recrystallization (DRX): one occurring at 950 °C and 0.001 s^{-1} with an efficiency of power dissipation of 37 pct and the other at 1200 °C and 0.1 s^{-1} with an efficiency of 40 pct. Dynamic recrystallization in the former domain is nucleated by the $\delta(Ni_3Nb)$ precipitates and results in fine-grained microstructure. In the high-temperature DRX domain, carbides dissolve in the matrix and make interstitial carbon atoms available for increasing the rate of dislocation generation for DRX nucleation. It is recommended that IN-718 may be hot-forged initially at 1200 °C and 0.1 s^{-1} and finish-forged at 950 °C and 0.001 s^{-1} so that fine-grained structure may be achieved. The available forging practice validates these results from processing maps. At temperatures lower than 1000 °C and strain rates higher than 1 s^{-1}, the material exhibits adiabatic shear bands. Also, at temperatures higher than 1150 °C and strain rates more than 1 s^{-1}, IN-718 exhibits intercrystalline cracking. Both these regimes may be avoided in hot-working IN-718.

I. INTRODUCTION

THE nickel-base superalloy IN-718* is used for several critical gas-turbine components, many of which are hot-forged. For obtaining required low-cycle fatigue and fracture properties, it is essential that the microstructure is controlled at the processing stage. For example, in the turbine disc application, a fine-grained structure is preferred for which the technology of forging and thermomechanical processing are described.[1,2] The hot ductility of IN-718 tested under tension in the temperature range of 1000 °C to 1050 °C reaches its peak value at a strain rate of about 2.5 s^{-1}.[3] Recently, Chaudhury *et al.*[4] have developed a processing map for hot deformation of IN-718 in the temperature range of 975 °C to 1150 °C and in the strain-rate range of 0.01 to 25 s^{-1} and interpreted the map in terms of dynamic recrystallization (DRX) mechanism and phase changes occurring in the material. As the commercial forging practice involves initial forging at high temperatures (>1150 °C) and finish forging below 980 °C to obtain fine-grained structures, it will be beneficial if data are obtained in wider temperature and strain-rate ranges. The purpose of the present investigation is to evaluate the hot deformation behavior in wide temperature and strain-rate ranges and generate a processing map for hot working of IN-718 with a view to optimizing its workability and microstructure during processing. Processing maps are developed on the basis of the dynamic materials model,[5] which is reviewed by Gegel *et al.*[6] and Alexander.[7] The model considers the workpiece as a dissipator of power, and the instantaneous power dissipated at a given strain rate ($\dot{\varepsilon}$) consists of two complementary parts: G content and J cocontent representing the temperature rise and microstructural dissipation, respectively. The factor that partitions power between J and G is the strain-rate sensitivity (m) of flow stress (σ). The J cocontent is given by[5]

$$J = \left(\frac{m}{m+1}\right)\sigma\dot{\varepsilon} \qquad [1]$$

where $\dot{\varepsilon}$ is strain rate. For an ideal linear dissipator, $J = J_{max} = \sigma \cdot \dot{\varepsilon}/2$ and the efficiency of power dissipation of a nonlinear dissipator may be expressed in terms of a dimensionless parameter:

$$\eta = \frac{J}{J_{max}} = \frac{2m}{(m+1)} \qquad [2]$$

The variation of η with temperature and strain rate constitutes the power dissipation map, the domains of which may be interpreted in terms of specific microstructural processes.

The extremum principles of irreversible thermodynamics as applied to large plastic flow[8] are applicable to the dynamic materials model. Kumar[9] and Prasad[10] combined these principles with those of separability of power dissipation and obtained a continuum criterion for obtaining flow instability during hot deformation, and it is given by

$$\zeta(\dot{\varepsilon}) = \frac{\partial \ln (m/m+1)}{\partial \ln \dot{\varepsilon}} + m < 0 \qquad [3]$$

The variation of the instability parameter $\zeta(\dot{\varepsilon})$ with temperature and strain rate is superimposed on the power dissipation map for delineating the regimes of flow instability where $\zeta(\dot{\varepsilon})$ is negative.

*IN-718 is a trademark of Huntington Alloys, Huntington, WV.

N. SRINIVASAN, Graduate Student, and Y.V.R.K. PRASAD, Professor and Chairman, are with the Department of Metallurgy, Indian Institute of Science, Bangalore 560012, India.

Manuscript submitted October 26, 1993.

II. EXPERIMENTAL

The chemical composition (wt pct) of IN-718 material used in this investigation is given in Table I. Cylindrical hot compression specimens of 8-mm diameter and 12-mm height were used. Concentric grooves of about 0.5-mm depth were engraved on the specimen faces to facilitate the retention of lubricant. A chamfer of 1 mm at 45 deg was machined along the edges of the face to avoid fold over in the initial stages of the compression. A 0.5-mm diameter hole was drilled to a depth of 4 mm at half the height of the specimen for insertion of a thermocouple.

Hot compression tests were conducted in the temperature range 900 °C to 1200 °C and in the strain-rate range of 0.001 to 100 s^{-1}. A computer-controlled servo-hydraulic machine (DARTEC, Stourbridge, West Midlands, UK) was used in this investigation. The machine could be operated with an exponential decay of actuator speed with time to give constant true-strain rate with strain. In arriving at the exponential decay equation for the stroke variation, the small elastic deflections of the machine and the grips were neglected. The accuracy of temperature controller was within ±2 deg and the adiabatic temperature rise during compression was measured with a thermocouple embedded in the specimen. From the load-stroke data, true stress–true strain values were calculated using standard equations. The flow stress data obtained at different temperatures and strain rates were corrected for the adiabatic temperature rise using linear interpolation of log σ *vs* $(1/T)$, and this correction was found to be significant at lower temperatures and higher strain rates. Power dissipation maps were constructed using these data. The following computational procedure was adopted for this purpose: log flow stress *vs* log strain-rate data at a constant temperature and strain were fitted using a cubic spline function, and the strain-rate sensitivity (m) was calculated as a function of strain rate. The procedure was repeated at different temperatures. The efficiency of power dissipation through microstructural changes $\eta = 2m/(m + 1)$ was then calculated from a set of m values as a function of strain rate and temperature and plotted as a three-dimensional (3-D) map. The 3-D variation of efficiency was projected as isoefficiency contour map onto the strain-rate temperature plane.

Specimens deformed under conditions of different domains were sectioned longitudinally (parallel to the compression axis) for optical metallographic examination. The cut surface was mechanically polished using standard techniques and etched electrolytically in a solution of 20 pct HCl and 80 pct methanol.

The tensile ductility of the material was measured using cylindrical specimens of 4-mm diameter and 25-mm gage length at different temperatures (900 °C to 1200 °C) and strain rates of 0.001 and 0.1 s^{-1}.

Table I. Chemical Composition (in Weight Percent) and Initial Grain Size of IN-718

Material	Chemical Composition (Wt Pct)	Initial Grain Size (μm)
IN-718	19.0Cr, 18.5Fe, 5.1Nb, 3.0Mo, 0.04C, 0.5Al, 0.9Ti, 0.2Si, Ni-balance	6

III. RESULTS

The initial microstructure of the material used in this investigation is shown in Figure 1, which exhibits fine-grained structure.

Typical true stress–true strain curves obtained at 950 °C and 1150 °C are shown in Figures 2(a) and (b). These represent typical behavior of the material at temperatures below and above the δ-phase dissolution temperature (1040 °C). The curves exhibit flow softening, which is significant at strain rates higher than 1 s^{-1}. The flow stress data corrected for adiabatic temperature rise are given in Table II, as a function of temperature, strain rate, and strain.

The power dissipation map obtained at a strain of 0.5 is shown in Figure 3. In this figure, the contours of isoefficiency (marked as percent) are projected onto a plane of temperature and strain-rate axes. The maps obtained at strains of 0.1, 0.2, 0.3, and 0.4 are essentially similar to that shown in Figure 3, indicating that strain does not have a significant influence. The map exhibits the following features:

(a) a domain occurring at temperatures below 1050 °C with a peak efficiency of 37 pct at 950 °C and 0.001 s^{-1};
(b) a domain occurring at temperatures above 1050 °C with a peak efficiency of about 40 pct occurring at 1200 °C and 0.1 s^{-1};
(c) a change in curvature of the contours occurring at 1050 °C; and
(d) in the high-temperature high-strain-rate corner of the map, the efficiency contours are closely spaced, indicating a sharp change in the efficiency values with increasing temperature and strain rate.

The instability map was developed on the basis of the continuum criterion given by Eq. [3] and is shown in Figure 4. The conditions under which the parameter $\zeta(\dot{\varepsilon})$ becomes negative are contoured and are shown as flow instability regimes (Figure 4). The material exhibits two such regimes at strain rates higher than 1 s^{-1}: one

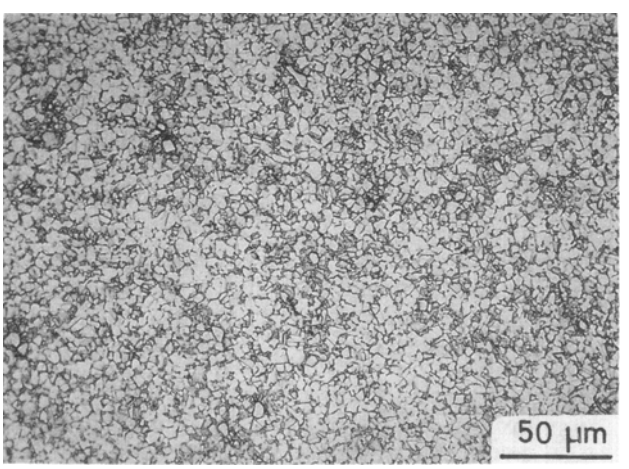

Fig. 1—Initial microstructure of the superalloy IN-718.

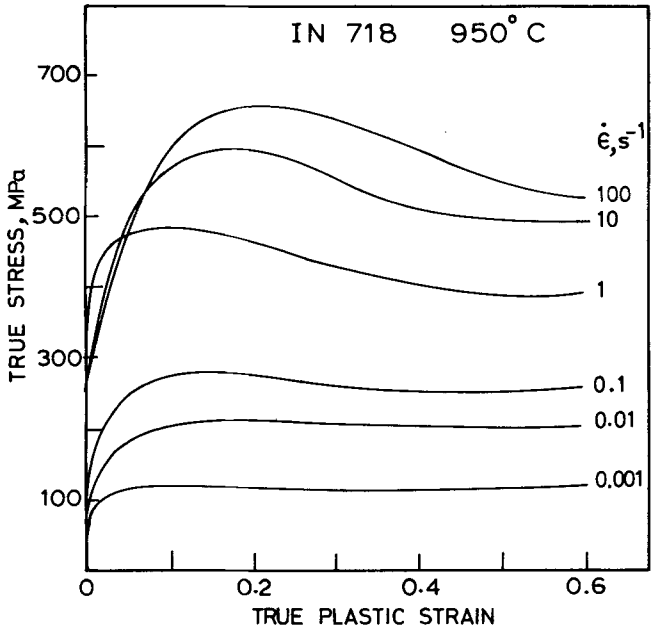

(*a*)

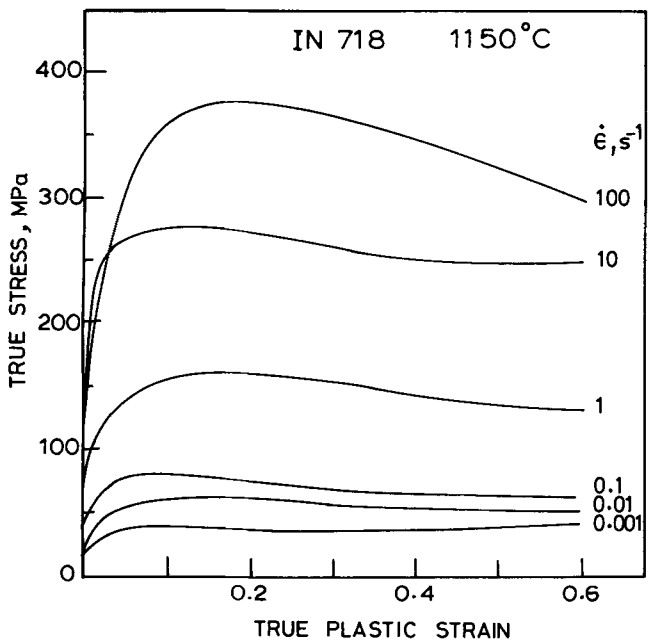

(*b*)

Fig. 2—(*a*) True stress–true plastic strain curves for IN-718 at 950 °C and at different strain rates. (*b*) True stress–true plastic strain curves for IN-718 at 1150 °C and at different strain rates.

occurring below about 1020 °C and the other occurring above 1120 °C. Specimens deformed in these regimes were examined for the microstructural manifestation of these two types of flow instabilities and are discussed in Section IV–A–3.

IV. DISCUSSION

The microstructure of IN-718 alloy has essentially a face-centered cubic (fcc)γ matrix, which is precipitation strengthened.[11] The major strengthening phase is γ'' precipitates (bct), which is coherent with the matrix. Some amount of ordered γ' precipitate (fcc) is also present in the matrix. In addition, δ phase with an ideal composition of Ni_3Nb having orthorhombic crystal structure is also present in IN-718. The δ phase occurs either as a blocky grain-boundary constituent or as Widmenstaten plates in the matrix. MC types of carbides are also present both in the matrix and along the grain boundaries.

The power dissipation characteristics of the specimen are dependent on the phases present at the temperature of deformation, and, therefore, solutionizing temperatures for the phases will be useful in interpreting the maps.

A. *Interpretation of Processing Map*

The processing maps are interpreted on the basis of the broad principle of atomistic mechanism represented in Raj maps.[12] The mechanisms considered are DRX and dynamic recovery, both of which are considered "safe" for processing. The limiting conditions which define the safe regime are obtained for fracture mechanisms like void formation dominating at lower temperatures and higher strain rates and wedge cracking occurring at higher temperatures and lower strain rates. The different domains exhibited by the power dissipation map may be identified on the basis of the corresponding efficiency variations, microstructural features, and ductility values. For example, the ductility in the dynamic recrystallization domain is high and the grain-size variation with temperature is sigmoidal. On the other hand, the domains representing fracture processes will exhibit poor ductility.

1. *Low-temperature domain*

The domain extends over a temperature range of 900 °C to 1020 °C at strain rates lower than 0.01 s^{-1} (Figure 3). The efficiency values of power dissipation exhibited by the domain are typical of the DRX process in nickel materials,[13,14] with its peak efficiency of 37 pct occurring at 950 °C and 0.001 s^{-1}. The flow curves obtained under different combination of strain rate and temperature in the domain show initial slight flow softening followed by a steady state (Figure 2(a)). This type of flow behavior has been widely accepted to result from the DRX process.[15] This is further confirmed on the basis of microstructural observations on the samples deformed under the conditions in the domain. Typical microstructures recorded on specimens deformed at a strain rate of 0.001 s^{-1} and at 900 °C, 950 °C, and 1000 °C are shown in Figures 5(a) through (c). These exhibit uniform fine recrystallized grain structures with serrated grain boundaries. The δ phase is effective in pinning the grain boundaries and in retaining a fine-grained structure. At temperatures above 1040 °C, grain growth is promoted (Figure 5(d)) since δ-phase dissolution occurs. In Figure 6, variations of ductility, average grain diameter, and efficiency of power dissipation with temperature in the DRX domain are compared. The ductility peak and the peak efficiency value occur at the same temperature (950 °C). The temperature at which 50 pct change in the grain size occurred in the sigmoidal variation of grain size (Figure 6(b)) has also coincided with the temperature of peak ductility and peak efficiency. This further

Table II. Flow Stress Values (in MPa) of IN-718 at Different Strain Rates and Temperatures (Corrected for Adiabatic Temperature Rise)

Strain	Strain Rate (s^{-1})	Temperature (°C)						
		900	950	1000	1050	1100	1150	1200
0.1	0.001	188	123	79.4	70.6	48.9	39	26.0
	0.01	293	210	134	104	87.3	60	51.4
	0.1	399	277	225	173	149	79.4	78.7
	1	616	486	332	258	215	156	136
	10	634	561	475	410	335	274	201
	100	684	598	546	509	417	354	217
0.2	0.001	185	123	79.4	72.8	50.4	36.8	24.1
	0.01	301	214	137	108	92.1	61.4	49.2
	0.1	394	281	221	177	153	75.6	74.6
	1	633	466	330	252	217	160	134
	10	711	601	459	406	340	273	182
	100	731	661	600	565	450	375	134
0.3	0.001	182	120	79	72.3	49.4	37.5	23.7
	0.01	308	212	132	112	83.4	58.3	46.5
	0.1	366	269	209	171	148	69.5	68.7
	1	587	435	317	235	208	154	127
	10	686	555	423	374	316	262	161
	100	691	639	571	545	432	365	60.7
0.4	0.001	173	118	81.5	73.4	50.9	38.4	23.5
	0.01	297	204	130	112	80.7	55.5	46.4
	0.1	348	261	201	166	141	65.8	64.0
	1	540	404	298	229	197	143	117
	10	638	512	392	354	295	251	144
	100	640	602	535	520	406	349	47.3
0.5	0.001	164	119	82.6	77.3	51.5	39.8	24.5
	0.01	294	203	131	113	80.4	53.3	47.6
	0.1	340	256	197	166	139	63.4	61.3
	1	512	392	280	235	190	135	108
	10	593	493	390	359	284	251	126
	100	600	561	493	500	378	327	37.5

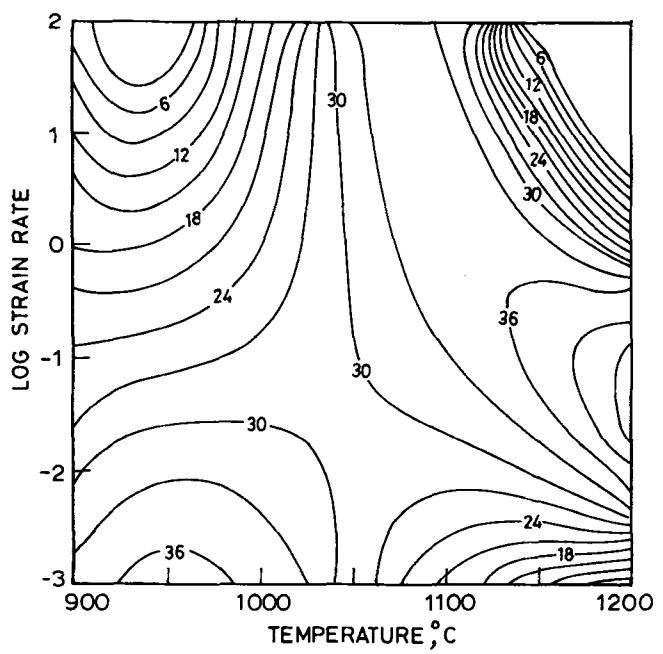

Fig. 3—Processing map for IN-718 at strain of 0.5. Numbers represent percent efficiency of power dissipation.

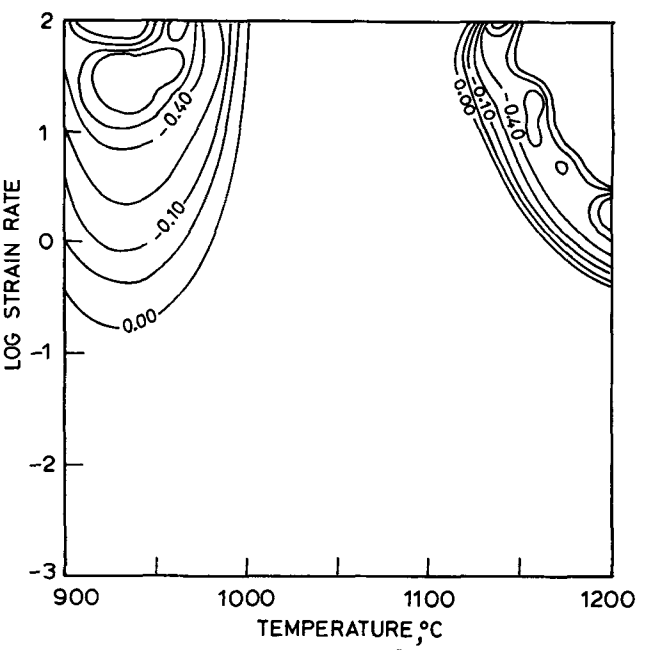

Fig. 4—Contour map of instability parameter $\zeta(\dot{\varepsilon})$ on temperature–strain rate plane for IN-718.

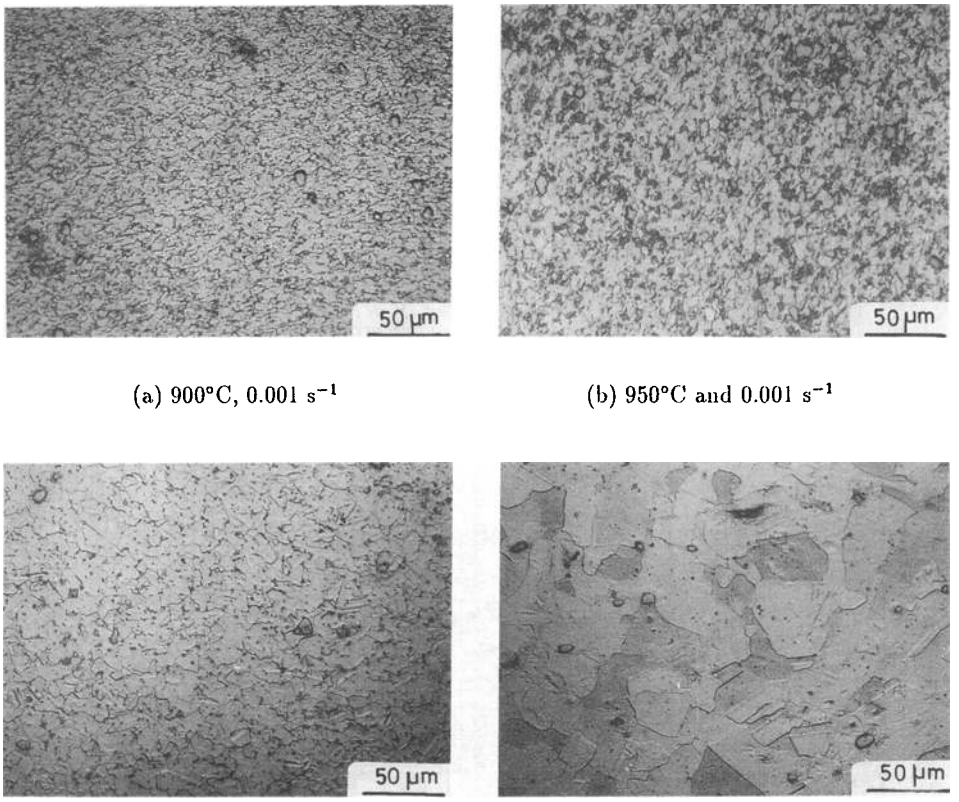

(a) 900°C, 0.001 s^{-1} (b) 950°C and 0.001 s^{-1}

(c) 1000°C and 0.001 s^{-1} (d) 1050°C and 0.001 s^{-1}

Fig. 5—Microstructures obtained on IN-718 specimens deformed at strain rate of 0.001 s^{-1} and at different temperatures: (*a*) 900 °C, (*b*) 950 °C, and (*c*) 1000 °C. These conditions correspond to lower temperature DRX domain. (*d*) Microstructure obtained on IN-718 specimen deformed at 1050 °C and 0.001 s^{-1} showing grain growth in the absence of δ precipitate.

corroborates with the interpretation that the domain represents the DRX process. In this domain, the grain-size variation (d) with steady-state flow stress (σ_s) is shown in Figure 7, which indicates a linear relationship between $(d)^{-15}$ and σ_s, as reported by others for the DRX process.[16]

2. *High-temperature domain*

This domain essentially occurs after the completion of δ dissolution. It extends over a strain-rate range of 0.01 to 0.5 s^{-1} at temperatures above 1150 °C, with its peak efficiency of 40 pct occurring at about 1200 °C and 0.1 s^{-1} (Figure 3). On the same lines of discussion for the low-temperature domain, this domain can also be interpreted to represent the DRX process. In this case, δ phase is not present in the matrix. In Figures 8(a) through (c), the microstructures obtained on samples deformed at 0.1 s^{-1} and across the domain at 1100 °C, 1150 °C, and 1200 °C are presented. Even though the grain sizes in this domain are much larger than that for the lower-temperature DRX domain, both domains have similar microstructural characteristics. The larger grain sizes in this high-temperature domain indicate that the carbides present in the matrix are not as effective as δ precipitates in hindering the grain-boundary migration. Further, the variations of ductility and the efficiency of power dissipation, as shown in Figures 9(a) and (c), are similar to that observed in the lower-temperature domain and confirm that the domain represents DRX. The continuous increase in the variations of average grain diameter with temperature (Figure 9(b)) indicates that the domain may extend even beyond 1200 °C. The mechanism of DRX in IN-718 both at lower and higher temperatures will be discussed in Section C.

3. *Instability regime*

The instability map (Figure 4) developed on the basis of the criterion given by Eq. [3] exhibits two distinct flow instability regimes occurring at higher strain rates (>1 s^{-1}) and at temperatures lower and higher than 1050 °C. The microstructural features of the instability are shown in Figure 10, which corresponds to the condition of 900 °C and 100 s^{-1}. The microstructure exhibits adiabatic shear bands oriented at about 45 deg with respect to the compression axis. In the case of higher strain rate (100 s^{-1}) of deformation, the shear band formation is so intense that fracture occurred along the band (Figure 10). When the rate of deformation is reduced, the shear band formation will be less intense and appears diffused. For the high-temperature instability regime, on the other hand, the microstructure exhibits intergranular cracking, as shown in Figure 11, which corresponds to a deformation condition of 1200 °C and 100 s^{-1}. This may be due to the presence of iron as well as coarse carbides at the grain boundaries, which causes fracture at high strain rates due to embrittlement of grain boundaries at higher temperatures.

The discussion on processing maps indicates that the initial forging steps are best done at 1200 °C and 0.1 s^{-1}

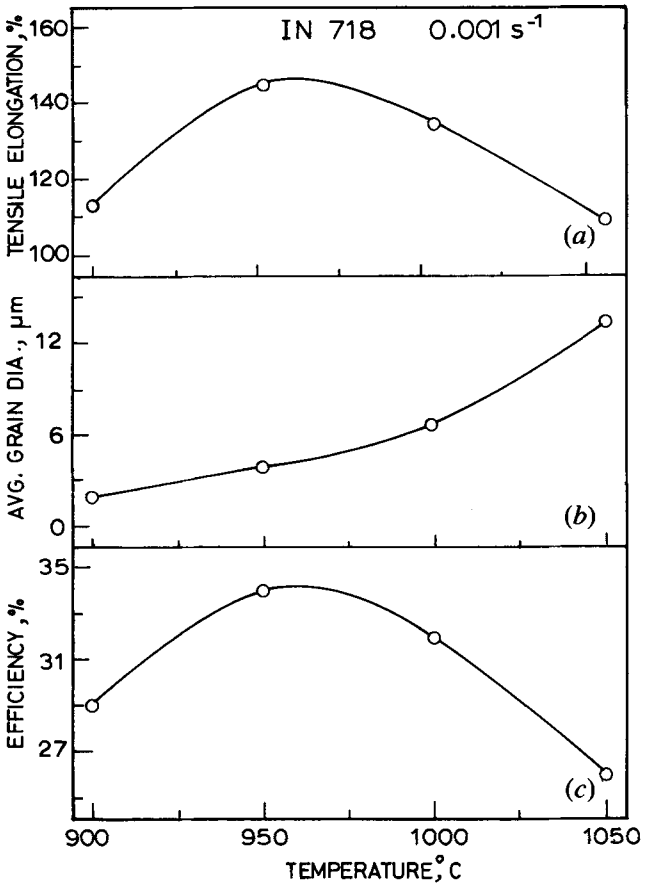

Fig. 6—Variations of (*a*) ductility, (*b*) average grain diameter, and (*c*) efficiency of power dissipation with temperature at strain rate 0.001 s^{-1} in lower-temperature DRX domain of IN-718.

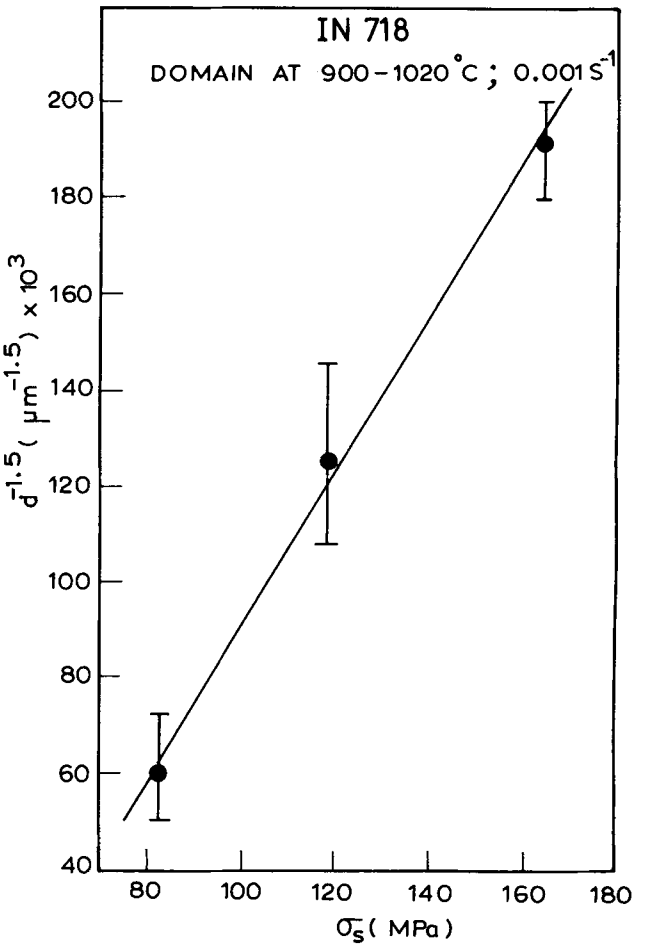

Fig. 7—Variation of grain size (d) with steady-state flow stress (σ_s) in the lower-temperature DRX domain.

(high-temperature DRX domain) (Figure 3), where the workability is high and the forging loads are low. As fine-grained microstructure is preferred for components like turbine disc, the finish forging may be conducted at 950 °C and 0.001 s^{-1} (lower-temperature DRX domain). The material offers two domains of DRX, and hence, considerable microstructural control may be achieved using processing maps.

4. *Processing—Microstructure correlation in IN-718*

In summary, the microstructural response of IN-718 to the processing parameters is shown schematically in Figure 12. Processing in the high-temperature DRX domain results in somewhat coarser grain structures, whereas the lower-temperature DRX domain gives fine-grained structure in the component. The later domain may be used for finishing operations. Strain rates higher than about 1 s^{-1} may be avoided for processing this material, because these lead to microstructural instabilities.

B. *Correlations with Earlier Studies*

The results of previous studies on microstructural mechanisms during hot deformation of IN-718[17,18] are compared with the present results of processing map. The DRX in IN-718 alloy has been reported to occur at 950 °C and at strain rates below 10^{-2} s^{-1} but not lower than 10^{-4} s^{-1}.[18] This result is in good accordance with the lower-temperature DRX domain of the processing map (Figure 3). Also, a nonuniform flow behavior with shear band formation observed at high strain rates (>1 s^{-1}) below the δ solvus temperature[17] is also in conformity with the instability conditions predicted by the map (Figure 4). The tensile ductility data obtained[3] at a nominal strain rate of 2.5 s^{-1} over a temperature range of 900 °C to 1200 °C, showed a maximum at 950 °C followed by a sharp ductility drop above 1100 °C. The increase in the ductility has been attributed to enhanced DRX, whereas the ductility drop has been attributed to δ precipitate coarsening. When this ductility variation is compared with the variation of efficiency of power dissipation at 2.5 s^{-1} in the temperature range of 900 °C to 1200 °C (Figure 13), a similar trend is observed in both the cases. However, from the processing map (Figure 3), it is inferred that the test condition (1050 °C and 2.5 s^{-1}) at which the maximum of ductility and efficiency occur falls between the two instability regimes (Figure 4) and that generally, the ductility values are lower in the instability regime than that in the stable region. Although the maximum ductility condition falls in the stable flow region predicted by processing map, it does not correspond to the optimum DRX conditions in either of the domains. Because this region corresponds to a "bifurcation" regime, microstructural control may be difficult to achieve. In another study by Chaudhury *et al.*[4] on

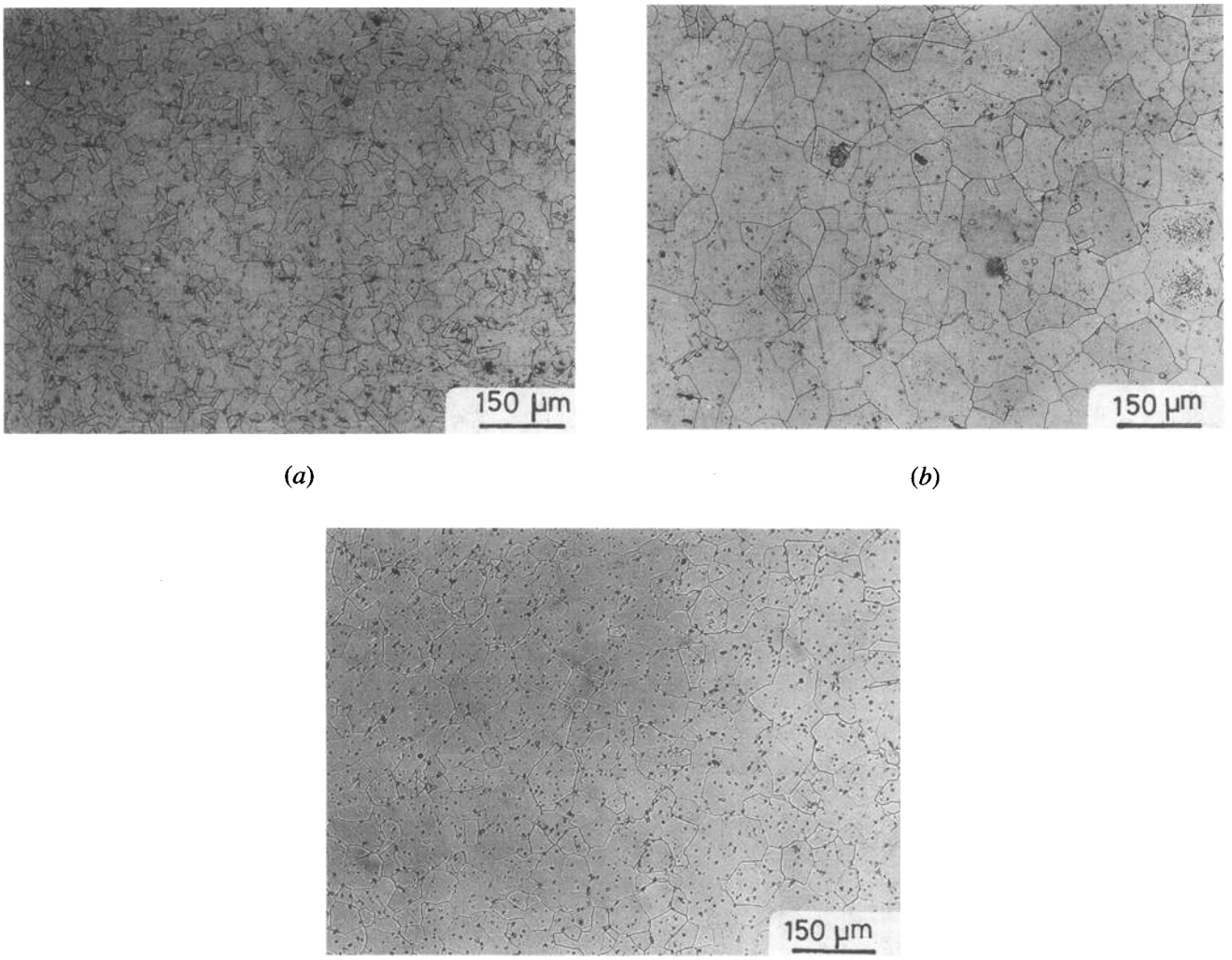

(*a*) (*b*) (*c*)

Fig. 8—Microstructures obtained on IN-718 specimens deformed at strain rate of 0.1 s^{-1} and at different temperatures: (*a*) 1100 °C, (*b*) 1150 °C, and (*c*) 1200 °C. These conditions correspond to higher-temperature DRX domain.

the process optimization of IN-718 in the temperature and strain-rate ranges of 975 °C to 1150 °C and 0.01 to 2.5 s^{-1}, DRX has been reported. However, when this temperature–strain rate frame is superimposed on the processing map (Figure 3), the test conditions used by Chaudhury *et al.* [4] do not cover optimum conditions for either of the DRX domains. Thus, optimization using these data may not, therefore, lead to useful results on microstructural control.

C. *Mechanism of DRX*

IN-718 exhibits two distinct DRX domains unlike pure nickel[13] and other nickel alloys, namely, Ni-20Cr[14] and IN-600.[19] The DRX conditions are greatly influenced by alloying elements as well as the various phases present in the material.[20] IN-718 being a nickel-iron-base alloy, the Ni-Cr-Fe system forms the matrix phase. As IN-600 basically consists of the Ni-Cr-Fe system with carbide precipitates, the characteristics of DRX process in IN-600[19] are compared with those of IN-718. IN-600 exhibits a single DRX domain with its peak occurring at the same temperature and strain-rate conditions (1200 °C and 0.1 s^{-1})[19] as the higher-temperature DRX domain of IN-718. In both these cases, the temperature range at which the DRX domain starts appearing has coincided with that of carbide dissolution. Further, the material NICHROME,* which forms the basic matrix of the Ni-Cr binary system for many NIMONIC** alloys, also exhibits a similar DRX domain[14] as IN-600 but over a wider range of temperature. This is because in IN-600, carbide dissolution occurs at lower temperatures. A striking difference in the DRX conditions are observed when the processing maps of these alloys are compared with the map of high-purity nickel (99.98 pct).[13] The DRX domain in these alloys occurs at higher temperature (1200 °C) and lower strain rate (0.1 s^{-1}). Table III summarizes the DRX conditions in the processing maps for different nickel materials.

*NICHROME is a trademark of Harrison Alloys, Inc., Harrison, NJ.

**NIMONIC is a trademark of Inc. Alloys International, Inc., Huntington, WV.

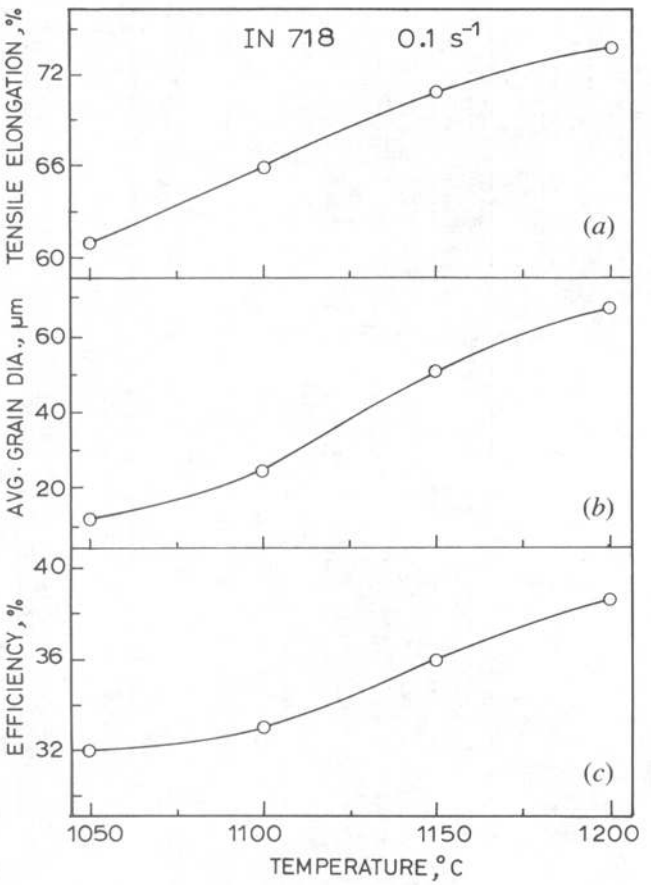

Fig. 9 — Variations of (*a*) ductility, (*b*) average grain diameter, and (*c*) efficiency of power dissipation with temperature at strain rate 0.01 s^{-1} in higher-temperature DRX domain of IN-718.

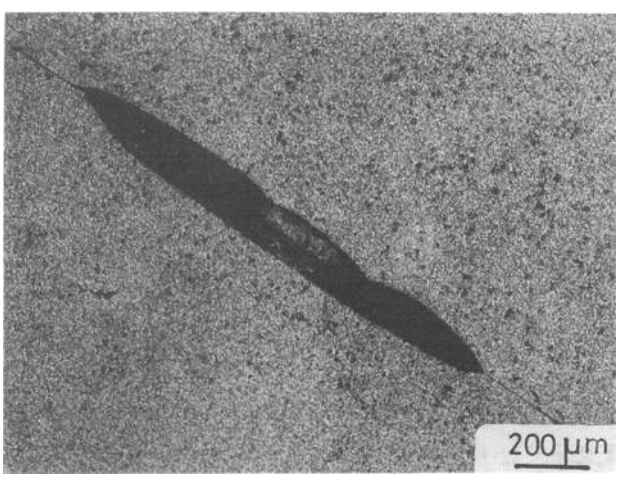

Fig. 10 — Microstructure obtained on IN-718 specimen deformed at 900 °C and 100 s^{-1} showing fracture along the adiabatic shear band. The compression axis is vertical.

At elevated temperatures, nickel has a lower stacking fault energy (SFE) (40 mJ/m^2 at 1000 °C)[21] and undergoes DRX at 925 °C and 1 s^{-1} with a peak efficiency of power dissipation of about 31 pct.[13] Also, the presence of carbon has a strong influence on the strain rate for DRX,[22] because interstitial carbon increases the rate of

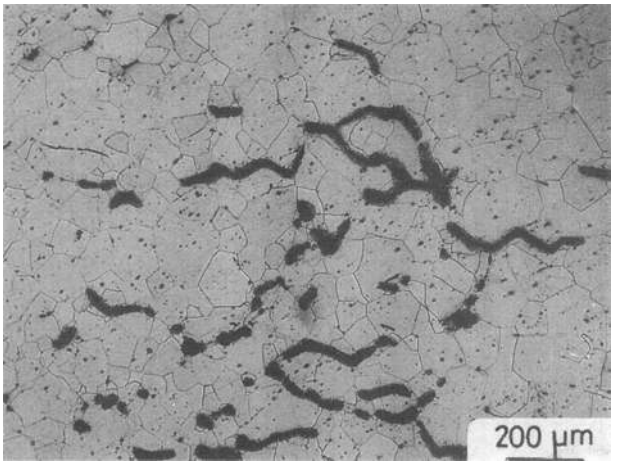

Fig. 11 — Microstructure obtained on IN-718 specimen deformed at 1200 °C and 100 s^{-1} showing intercrystalline cracking.

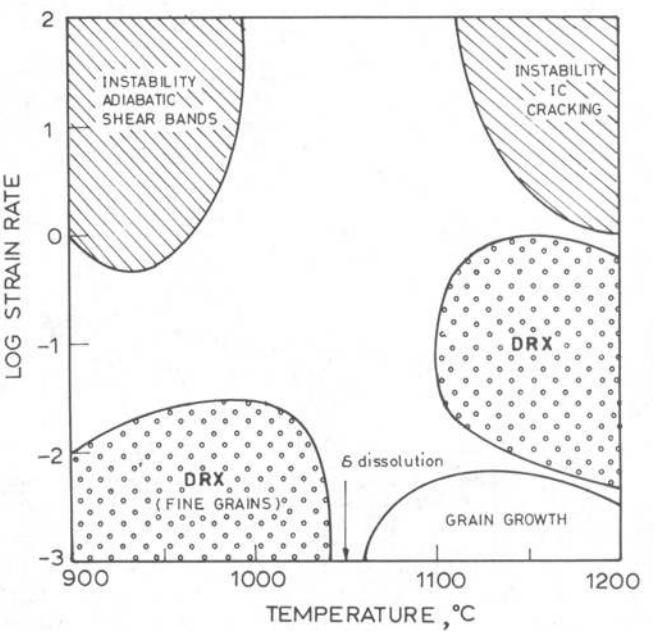

Fig. 12 — Various domains of microstructural mechanisms exhibited by IN-718 in the hot-working range as predicted by processing map.

dislocation generation. On the other hand, the addition of chromium lowers the SFE, and the nickel-base alloys may be considered to be low SFE materials.[23] Further, chromium in nickel causes strengthening due to long range stress fields, which in turn increase the DRX temperature.[14] The mechanism of DRX may be discussed on the basis of a simple DRX model, which considers the rate of nucleation *vs* the rate of grain-boundary migration. The nucleation consists of the formation of interfaces due to dislocation generation and simultaneous recovery and rearrangement. Unlike static recrystallization (SRX), in DRX, the dislocation generation and recovery processes occur simultaneously, leading to the formation of interface or subgrain. This interface will become a nucleus for DRX when it attains a critical configuration of a high-angle boundary and will grow by the

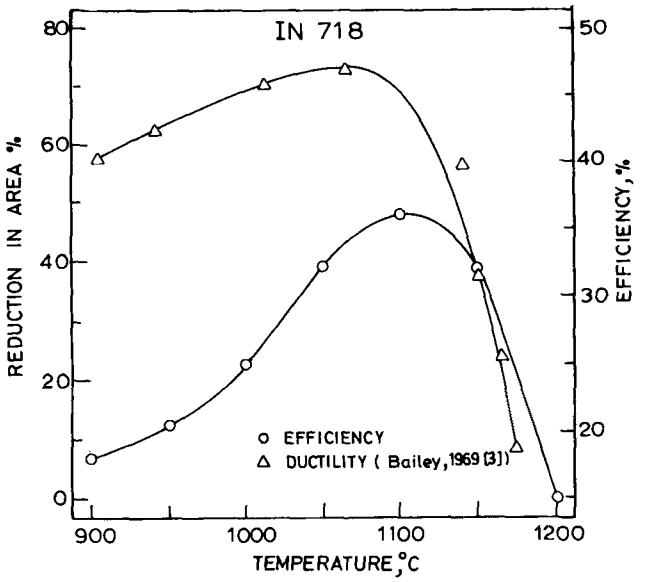

Fig. 13 — Variations of ductility[3] and efficiency of power dissipation with temperature at strain rate of 2.5 s^{-1} in IN-718.

Table III. DRX Temperature, Strain Rate, and Efficiency of Power Dissipation of Nickel Materials

	DRX		
Material	Temperature (°C)	Strain Rate (s^{-1})	Efficiency (Pct)
Nickel (99.98)	925	1.0	31
Ni-0.02C	925	0.0003	44
Ni-0.02C-0.002S	875	0.0003	46
Ni-20Cr	1200	0.1	38
IN-600	1200	0.2	48

process of migration. The driving force for interface migration in DRX is the reduction in the total energy for interfaces, whereas in SRX, it is the stored energy of individual dislocations. The nucleation rate R_F depends on the rate of generation of dislocation and the probability of their recovery:

$$R_F = \frac{\dot{\varepsilon}}{bl} \exp(-Q_D/RT) \quad (4)$$

The rate of annihilation of recovered groups of dislocations (subgrains) caused by migration of interfaces, R_M, may be assumed to be proportional to grain-boundary mobility M, and it is given by

$$R_M = C \cdot M \quad (5)$$

where C is a constant (10^{-6} m^{-1}) and M is given by the equation

$$M = D\Gamma/kTb \quad (6)$$

It was shown that in nickel, R_F is four orders of magnitude less than R_M at the peak DRX condition (925 °C and 1 s^{-1}).[13] Therefore, the rate of DRX nucleation in these materials is controlled by the diffusion-dependent climb of edge dislocations.

At lower temperatures (<1050 °C), the presence of δ phase in IN-718 promotes DRX nucleation by increasing the rate of dislocation generation. Therefore, lower strain rates (<0.01 s^{-1}) are sufficient to generate the required rate of dislocation density for the nucleation process of DRX. In contrast, it may be noted that the lower-temperature DRX domain is absent in NICHROME[14] and IN-600[19] materials because δ phase is not present in these alloys. On the other hand, DRX in these alloys occurs only at higher temperatures (1200 °C) and at strain rate 0.1 s^{-1}, as also in IN-718. At these high temperatures, the carbides (MC) go into solution and make interstitial carbon available for enhancing the nucleation rates for DRX. Carbon as an interstitial is very effective in increasing the rate of dislocation generation. Thus, it is clear that carbide dissolution precedes the occurrence of DRX in all these alloys.

The peak efficiency of power dissipation in IN-718 is lower than that in IN-600 but slightly higher than that in NICHROME. It is likely that the presence of Chromium,[24] niobium, and molybdenum in solution in IN-718 at 1200 °C decreases the rate of climb and hence the rate of DRX nucleation. This is counteracted by the increase in the climb rate due to the lower activation energy for diffusion of chromium in Nickel caused by the presence of iron.[25] Thus, in IN-718, the DRX efficiency lies between that of IN-600 and NICHROME, although all other parameters remain essentially unchanged.

D. *Recommended Forging Practice*

The forging sequence for IN-718 given by Marsh[2] has two stages of operation: initial forging, above the δ solutionizing temperature, and final forging, below the δ solutionizing temperature. By comparing this with the processing map Figure 3 that exhibits change in curvature of the power dissipation contours at the temperature of completion of δ dissolution (1040 °C), the following inferences may be made:

the initial phase of forging conditions correspond to the conditions of the higher-temperature domain; and
the final phase of forging conditions correspond to the conditions of lower-temperature domain.

Both these domains represent the DRX process, which is considered to impart good workability during forming operation[26] and produces more uniform microstructure throughout the component. As the grain growth is inhibited by δ precipitate, the finish forging carried out in the lower-temperature DRX domain results in fine-grain recrystallized structure. The temperature used[27] (<1040 °C) for final forging of IN-718 falls within this domain. However, unlike the forging temperature, the forging speed, which is also a critical parameter in thermomechanical processing, is not well documented in the literature. It is evident from the processing map that the two DRX domains have a shift of nearly two orders of magnitude on the strain-rate scale. As discussed in Section IV–A–3, the higher strain rates, at lower temperatures, lead to adiabatic shear band formation, whereas at higher temperatures, they lead to intergranular cracking. Also, lower strain rates at higher temperatures (>1050 °C) lead to abnormal grain growth resulting in

poor workability with low efficiency values of power dissipation. Therefore, the optimum conditions for the forging sequence provided by the processing map are as follows:

(a) initial forging at 1200 °C and 0.1 s^{-1} with δ phase in solution, and
(b) final forging at 950 °C and 0.001 s^{-1} in the presence of δ phase.

In order to control the microstructures of the component closely, it is necessary that each of these steps be conducted, limiting the processing conditions to within each of the domain.

V. CONCLUSIONS

The hot-working characteristics of IN-718 are studied in the temperature range 900 °C to 1200 °C and strain-rate range 0.001 to 100 s^{-1} using processing maps. The following conclusions are drawn from this investigation.

1. IN-718 exhibits two domains of DRX, one with a peak efficiency of 38 pct occurring at 950 °C and 0.001 s^{-1} and the other with a peak efficiency of 40 pct occurring at 1200 °C and 0.1 s^{-1}.
2. The DRX at lower temperatures is nucleated by δ phase (Ni_3Nb), whereas interstitial carbon present due to carbide dissolution causes DRX at higher temperatures. Fine grain size is produced during forging at 950 °C because of the presence of δ precipitates.
3. Hot working in the initial stages is best done at 1200 °C and 0.1 s^{-1} and finishing operations are done in the lower-temperature DRX domain so that fine grain size is achieved.
4. The material exhibits flow instabilities in the form of adiabatic shear bands at temperatures lower than 1000 °C and higher than 1 s^{-1}.
5. Intercrystalline cracking occurs at temperatures higher than 1150 °C and strain rates higher than 1 s^{-1}.

REFERENCES

1. *Metallurgy and Applications of Superalloy 718*, Edward A. Loria, ed., TMS-AIME, Warrendale, PA, 1989.
2. A.E. Marsh: *Metallurgia*, 1982, vol. 49, pp. 10-20.
3. R.E. Bailey: Report No. SP-69-9, Allegheny Ludlum Steel Research Center, Brackenridge, PA, 1969.
4. P.K. Chaudhury, J.J. Valencia, and D. Zhao: *Materials Week '92*, ASM and TMS, Chicago, IL, p. 65 (Abstract).
5. Y.V.R.K. Prasad, H.L. Gegel, S.M. Doraivelu, J.C. Malas, J.T. Morgan, K.A. Lark, and D.R. Barker: *Metall. Trans. A*, 1984, vol. 15A, pp. 1883-92.
6. H.L. Gegel, J.C. Malas, S.M. Doraivelu, and V.A. Shende: *Metals Handbook*, ASM, Metals Park, OH, 1987, vol. 14, pp. 417-38.
7. J.M. Alexander: *Modelling of Hot Deformation of Steels*, Springer-Verlag, Berlin, 1989, pp. 101-14.
8. H. Ziegler: *Progress in Solid Mechanics*, John Wiley and Sons, New York, NY, 1963, vol. 4, pp. 93-193.
9. A.K.S. Kalyan Kumar: Master's Thesis, Indian Institute of Science, Bangalore, 1987.
10. Y.V.R.K. Prasad: *Ind. J. Technol.*, 1990, vol. 28, pp. 435-51.
11. C.T. Sims and W.C. Hagel: *The Superalloy*, Wiley-Interscience Publishing, New York, NY, 1972.
12. R. Raj: *Metall. Trans. A*, 1981, vol. 12A, pp. 1089-97.
13. N. Srinivasan and Y.V.R.K. Prasad: *Mater. Sci. Technol.*, 1992, vol. 8, pp. 206-12.
14. N. Srinivasan and Y.V.R.K. Prasad: *J. Mater. Process. Technol.*, 1994, vol. 41, pp. 409-24.
15. M.J. Luton and C.M. Sellars: *Acta Metall.*, 1969, vol. 17, pp. 1033-43.
16. H.J. McQueen and J.J. Jonas: *Treatise Mater. Sci. Technol.*, 1975, vol. 6, pp. 393-493.
17. T.E. Howson and W.J. Couts, Jr.: *Metallurgy and Applications—Superalloy 718*, TMS-AIME, Warrandale, PA, 1989, pp. 685-94.
18. P.E. Mosser, G. Leconte, J. Leray, A. Lasalmonie, and Y. Honnarat: *Metallurgy and Applications—Superalloy 718*, TMS-AIME, Warrandale, PA, 1989, pp. 79-93.
19. N. Srinivasan and Y.V.R.K. Prasad: *Mater. Sci. Technol.*, in press.
20. M. Ueki, S. Horie, and T. Nakamura: *Mater. Sci. Technol.*, 1987, vol. 3, pp. 329-37.
21. M.N. Shetty and A.K. Laha: *Z. Metallkd.*, 1986, vol. 6, pp. 397-402.
22. N. Srinivasan and Y.V.R.K. Prasad: Indian Institute of Science, Bangalore, unpublished research, 1993.
23. B.E.P. Beeston and L.K. France: *J. Inst. Met.*, 1968, vol. 96, pp. 105-07.
24. K. Monma; H. Suto, and H. Oikama: *J. Jpn. Inst. Met.*, 1964, vol. 28, pp. 188-96.
25. D.D. Pruthi, M.S. Anand, and R.P. Agarwala: *J. Nucl. Mater.*, 1977, vol. 64, pp. 206-10.
26. W.J. McG. Tegart: *Ductility*, ASM, Metals Park, OH, 1968, pp. 133-77.
27. W.A. Wilkinson: *Metallurgy and Applications—Superalloy 718*, TMS-AIME, Warrandale, PA, 1989, pp. 119-34.